Surfaces and Interfaces 64 (2025) 106376

Contents lists available at ScienceDirect

Surfaces and Interfaces

journal homepage: www.sciencedirect.com/journal/surfaces-and-interfaces

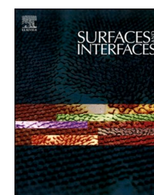

Effect of exposing Se pre-implanted polycrystalline SiC to maximum electronic energy loss of 33.7 keV/nm and annealing

T.S. Mabelane [a,*], Z.A.Y. Abdalla [a], V.A. Skuratov [b,c,d], S.S. Ntshangase [e], S.C. Masikane [f], T.T. Hlatshwayo [a]

[a] Physics Department, University of Pretoria, Pretoria, South Africa
[b] Joint Institute for Nuclear Research, Dubna, Russia
[c] Dubna State University, Dubna, Moscow Region, Russia
[d] National Research Nuclear University MEPhI, Moscow, Russia
[e] Department of Physics, University of Zululand, P/B X1001, KwaDlangezwa 3886, South Africa
[f] Department of Chemistry, University of Zululand, P/B X1001, KwaDlangezwa 3886, South Africa

ARTICLE INFO

Keywords:
SiC
Implantation
Se
SHIs
Annealing
Recrystallization

ABSTRACT

In this work the effect of swift heavy ions (SHIs) (710 MeV Bi^{51+}) irradiation and annealing on selenium (Se) pre-implanted silicon carbide (SiC) was investigated. SiC samples were implanted individually with 200 keV Se ions to a fluence of 1×10^{16} cm^{-2} at both room temperature (RT) and 350 °C. Following this, some pre-implanted samples were irradiated at RT with 710 MeV Bi^{51+} ions to a fluence of 1×10^{13} cm^{-2}. These irradiated samples then underwent sequential annealing at temperatures ranging from 1000 to 1200 °C, in 100 °C increments, for 10 h. The samples were characterized using Raman, SEM, TEM, and RBS. Sequential annealing of the RT pre-implanted and then irradiated sample up to 1200 °C led to recrystallization of the highly defective SiC layer into strained nano-crystalline SiC with cavities, accompanied by the formation of Se precipitates. In contrast, sequential annealing of the 350 °C pre-implanted and then irradiated sample up to 1200 °C also caused recrystallization of the defective SiC layer into nano-crystalline SiC, but with minor strained regions. No loss or migration of Se was detected in either the RT or 350 °C pre-implanted samples following SHIs irradiation and annealing up to 1200 °C.

1. Introduction

The global pursuit of clean and sustainable energy is essential for significantly reducing greenhouse gas emissions, minimizing air pollution, and combating climate change. This drive has sparked worldwide interest in pioneering Generation IV nuclear reactors, which are among the most promising solutions for clean energy. These reactors are designed to optimize thermal output while minimizing the release of harmful radioactive fission products (FPs).

Among the various design options for Generation IV reactors, the high-temperature gas-cooled reactor (HTGR) is notable for its use of tri-structural isotropic (TRISO) fuel particles. These coated particles are engineered to effectively contain radioactive FPs. A TRISO fuel particle is composed of layers of carbon (C) and silicon carbide (SiC) that are deposited via chemical vapor deposition (CVD) to encapsulate the fuel kernel (UO_2) [1,2]. The SiC layer in TRISO particle acts as the primary diffusion barrier for most metallic FPs, owing to its remarkable properties such as exceptional hardness, extremely low diffusion of impurities, outstanding resistance to high temperatures, with significant decomposition only beginning at 1700 °C, and small neutron absorption cross section [2–5]. These outstanding characteristics ensure the integrity of the TRISO fuel particle under extreme conditions, making it a reliable containment mechanism for FPs even in potential accident scenarios [1].

In the core of a TRISO particle, a uranium isotope (U-235) captures a slow-moving neutron, which destabilize the nucleus and causes it to split into two lighter FPs, releasing two or three neutrons and a substantial amount of energy. The energy range of FPs varies from low keV to 100 MeV (analogous to the energy levels of swift heavy ions (SHIs)). Consequently, during the operation of a fission nuclear reactor, SiC will also be subjected to FPs of energies of keV and 100 MeV at elevated temperatures. When SHIs traverse a material, they primarily lose energy

* Corresponding author.
E-mail address: u22019937@tuks.co.za (T.S. Mabelane).

https://doi.org/10.1016/j.surfin.2025.106376
Received 15 November 2024; Received in revised form 14 March 2025; Accepted 1 April 2025
Available online 2 April 2025
2468-0230/© 2025 The Author(s). Published by Elsevier B.V. This is an open access article under the CC BY-NC license (http://creativecommons.org/licenses/by-nc/4.0/).

through electronic interactions at higher energies. As they slow down to lower keV energies, energy loss shifts to nuclear interactions with the target nuclei. Therefore, to fully understand the microstructural evolution of SiC during nuclear reactor operation, it is essential to investigate the effects of irradiation from both slow/keV ions and SHIs at high temperatures mimicking the nuclear reactor environment.

Previous studies [6–15] have primarily focused on the effects of SHIs irradiation on SiC that had been pre-implanted with slower ions. Most of these investigations examined SHIs with maximum electronic energy losses of up to 20 keV/nm [6–10,14,15]. In contrast, only a few studies have explored the effects of SHIs with maximum electronic energy losses exceeding 20 keV/nm [11–13]. These studies primarily focused on the structural alterations of the substrate and transport mechanisms of the pre-implanted species.

The results indicated that keV ion implantation at room temperature (RT) amorphized SiC, while implantation at temperatures above the critical amorphization threshold (> 300 °C) preserved the original structure of SiC with defects. SHIs irradiation of RT-implanted SiC led to epitaxial recrystallisation from the amorphous-crystalline (a-c) interface, resulting in the formation of nanocrystalline SiC embedded within the amorphous matrix [6,7,9,13]. Furthermore, SHIs irradiation of SiC implanted at temperatures above the critical amorphization threshold resulted in nearly complete recrystallization [13,15]. Notably, no migration of pre-implanted species was observed following SHIs irradiation in any of the pre-implanted SiC samples.

To the best of our knowledge, the effects of high-temperature annealing have only been investigated for SiC pre-implanted with slow ions and subsequently irradiated with SHIs having a maximum electronic energy loss of 20 keV/nm [6–8]. No studies have reported on annealing for pre-implanted SiC irradiated with SHIs having electronic energy losses greater than 20 keV/nm.

Selenium (Se) is a significant fission product with important implications for reactor safety and waste management [16]. Se-79, a long-lived beta-emitting isotope found in spent nuclear fuel, poses potential risks to humans and the environment [17–19]. Therefore, effective containment of Se in TRISO particles is critical. Recent studies have primarily examined the impact of annealing on the microstructural properties of Se-implanted SiC and the migration behavior of Se within this material [16,20,21]. Additionally, recent work by ref [13] has investigated the effects of SHIs on the structural evolution of Se pre-implanted SiC, as well as the migration of Se within the SiC matrix. Investigating the behavior of Se within polycrystalline SiC, particularly after high-electronic energy loss exposure and subsequent annealing, is vital for assessing the integrity of TRISO particles under extreme conditions.

This study also seeks to bridge the existing knowledge gap by examining the effects of SHIs irradiation and subsequent annealing on pre-implanted polycrystalline SiC. By irradiating Se pre-implanted polycrystalline SiC with 710 MeV Bi^{51+} ions, we will analyze how the combination of high electronic energy loss (33.7 keV/nm) and thermal treatment influences defect formation, migration behavior, and the overall microstructure of SiC. Additionally, the findings will be contextualized with previous research on Se-implanted SiC [16], which indicated that heat treatment can lead to significant structural changes, including recrystallization and the migration of Se ions, depending on the implantation temperature and annealing conditions. Moreover, the results of these study will also be compared with similar annealing studies of pre-implanted SiC irradiated with SHIs of 20 keV/nm, as reported in [6–8].

This research will contribute to a deeper understanding of SiC's durability under extreme conditions and provide valuable insights for developing strategies to efficiently contain Se-79, a long-lived radioactive isotope that poses a significant challenge in nuclear waste management.

2. Experimental method

Polycrystalline SiC wafers, primarily consisting of the 3C-SiC polytype with some traces of 6H-SiC polytype, were the starting material in this study [13,22]. The pristine SiC were implanted with 200 keV Se ions, under two conditions: at RT and 350 ℃ (slightly above critical amorphization threshold temperature), to a fluence of 1×10^{16} cm^{-2} at the Friedrich-Schiller-University Jena, Germany. Afterward, the pre-implanted SiC samples were irradiated with 710 MeV Bi^{51+}at RT to a fluence of 1×10^{13} cm^{-2} utilizing IC-100 FLNR cyclotron. Further experimental details of both implantation and irradiation can be found in ref [13]. The implanted and then irradiated samples underwent sequential annealing using a computer-controlled Webb 77 graphite furnace at temperatures ranging from 1000 to 1200 °C in 100 °C intervals, each for a duration of 10 h as elaborated in ref [16].

RBS was used to monitor the migration of implanted Se ions both before and after annealing. The analysis was performed using 2 MeV helium (He^{+}) ions, with a silicon (Si) surface barrier detector placed at a scattering angle of 150° to detect the backscattered ions. The experiment was conducted at a constant current of around 500 pA, collecting a total charge of 500 nC for each measurement. The Ziegler, Biersack, and Littmark (ZBL) stopping powers were applied to convert the RBS spectra from channel numbers to depth (in nm). The surface morphological changes of SiC were examined with a Zeiss Ultra 55 field emission gun scanning electron microscope (FEG-SEM) equipped with an in-lens detector and operated at an acceleration voltage of 2 kV. The structural evolution was monitored with Witec alpha 300 RAS+ Raman spectrometer, utilizing a 532 nm green laser at a power output of 2.5 mW. Further details about the characterization techniques used in this work was extensively discussed in ref [13]. Additionally, the microstructural evolution following annealing were examined using transmission electron microscopy (TEM), with cross-sectional TEM lamellae prepared as detailed in ref [13]. The TEM micrographs were captured using a Jeol F200 Multi-Purpose Electron Microscope equipped with a Gatan Rio camera and Oxford X-MaxN 80 T Energy Dispersive X-ray Spectroscopy (EDS) detector. Imaging and micro-elemental analyses were conducted at an accelerating voltage of 200 kV and EDS data was captured and processed using the AZtec software suite.

3. Results and discussions

Prior to implantation and irradiation, simulations of Se and Bi ions were conducted using stopping and range of ions in matter (SRIM) 2012 in full cascade mode, as described in ref [13]. Fig. 1 shows the relative atomic density (RAD) (%) and displacement per atom of Se ions and 710 MeV Bi^{51+} ions implanted/ irradiated into SiC as function of depth. Additionally, the electronic energy loss of 710 MeV Bi^{51+} as function of depth is also shown. The inset in Fig. 1(a) provides a zoomed-in view highlighting the amorphization threshold. RAD (%) and displacement per atom (dpa) were calculated as discussed in ref [13]. The simulations predicted that 200 keV Se ions implantation into SiC induces an amorphous layer of approximately 150 nm thick, with a projected range at a depth of 89.6 nm, while 710 MeV Bi^{51+} ions do not amorphize the SiC as extensively discussed in ref [13] (see to Fig. 1(a) and (b)). Experimental depth profiles from RBS for Se ions implanted into SiC at RT and 350 °C were nearly Gaussian, with projected ranges that closely aligns with the simulated [13]. The simulations further revealed that 200 keV Se ions primarily lose energy through nuclear interactions within SiC, with a maximum nuclear energy loss of 1.73 keV/nm. In contrast, 710 MeV Bi^{51+} ions predominantly lose energy via electronic interactions, with a maximum electronic energy loss of 33.7 keV/nm, which is most dominant near the surface, as detailed in ref [13].

Fig. 2 shows the Raman spectra of pristine SiC, as-irradiated and annealed (1000–1200 °C) samples along with their corresponding magnified view of LO peaks. The pristine and as-irradiated SiC spectra included in Fig. 2 are for comparison and are briefly discussed here, as

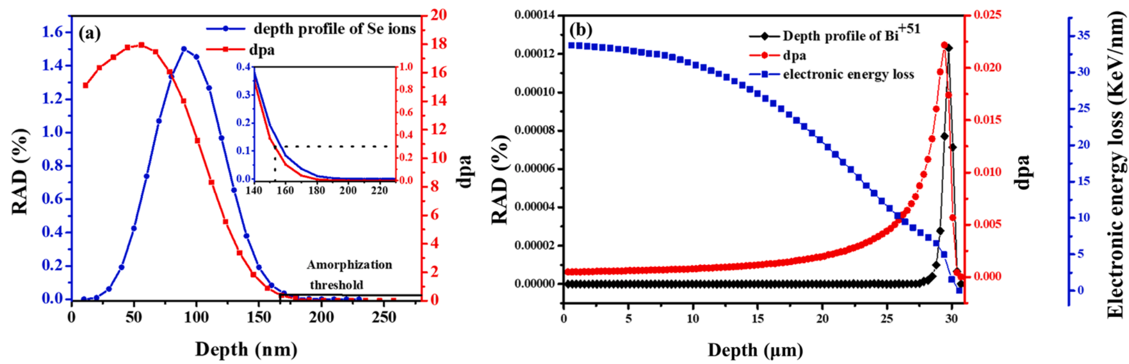

Fig. 1. SRIM simulation results showing the depth profile and displacements per atom (dpa) as a function of depth for (a) Se ions and (b) 710 MeV Bi^{51+}ions. Panel (b) also includes the electronic energy loss versus depth for the 710 MeV Bi^{51+} ions. The inset in (a) provides a zoomed-in view highlighting the amorphization threshold.

they were thoroughly analyzed in studies [13,16,23]. The pristine spectrum exhibits the Raman characteristic peaks of SiC within the wavenumber range of 700 to 1100 cm^{-1} as detailed in refs [13,16,23]. RT implantation caused partial loss of SiC characteristic peaks, along with the emergence of a Si-Si peak around 525 cm^{-1} and C—C peak around 1425 cm^{-1}, indicating amorphization of the SiC structure. In contrast, implantation at 350 °C, which is above the critical amorphization threshold for SiC (~300 °C) [1], resulted in the intensity reduction of the Raman SiC characteristic peaks, suggesting no amorphization but rather the accumulation of defects. Irradiation of the RT pre-implanted SiC with 710 MeV Bi^{51+} ions led to partial reappearance of the characteristic Raman peaks of SiC, while peaks around 525 cm^{-1} and 1425 cm^{-1} remained [13] (also see Fig. 2). This suggests limited recrystallization of the initially damaged SiC due to thermal spikes generated by the substantial electronic energy loss (33.7 keV/nm) of the 710 MeV Bi^{51+} ions. Irradiation of the 350 °C pre-implanted SiC with 710 MeV Bi^{51+} ions also led to recovery/recrystallization of some initially retained defects [13]. Annealing at 1200 °C for both RT and 350 °C pre-implanted and then irradiated samples led to the emergence of a small peak around 1350 cm^{-1}. This peak is likely associated with the formation of carbon-rich phases, resulting from partial thermal decomposition of the substrate.

Sequential annealing the SiC pre-implanted at RT then irradiated with, 710 MeV Bi^{51+} from 1000 to 1200 ℃ led to reappearance of SiC characteristic peaks, along with disappearance of both Si-Si and C-C peaks indicating significant recrystallization of the former amorphous SiC layer. These findings are partially consistent with earlier studies [6–8], where RT-implanted SiC was subjected to a maximum electronic energy loss of 20 keV/nm at fluences of 3.4×10^{14} cm^{-2} and 8.4×10^{14} cm^{-2}, followed by sequential annealing at high temperatures (1100-1500 ℃ in steps of 100 ℃). However, in these previous studies, annealing up to 1200 ℃ did not result in the vanishing of the Si-Si vibration mode. This may be due to the greater damage caused by the implanted species (Ag and Sr) compared to Se, along with the exposure of amorphous SiC to greater electronic energy loss from SHIs in this current work. In addition, the velocity of swift heavy ions significantly affects their interaction with the SiC substrate, as higher ion velocities are associated with a broader distribution of electronic excitations, as described in studies such as refs [24,25]. The velocity (v) is proportional to $\sqrt{2E/m}$, where E represents the kinetic energy and m the ion mass. Consequently, the higher energy of the 710 MeV Bi^{51+} ions ($v = 2.56 \times 10^7 m/s$) translates to a greater v compared to the 167 MeV Xe ions ($v = 1.57 \times 10^7 m/s$). In the case of 710 MeV Bi ions, the greater velocity likely results in a more extensive region of energy deposition compared to 167 MeV Xe ions. This distinction may explain the observed differences in defect recovery and recrystallization behaviour in our experiments. Sequential annealing the 350 ℃ implanted SiC then irradiated sample led to an increase in the intensity of SiC Raman characteristic peaks, indicating the recrystallization of defects.

To further investigate the crystallinity and stress evolution in Se pre-implanted SiC then irradiated, subsequently annealed from 1000 to 1200 ℃, the relative Raman intensity (RRI) and the average stress in the samples were calculated. The RRI was calculated utilizing equation (1) [26]:

$$RRI = \frac{I_{defective}}{I_{crystalline}} \tag{1}$$

Where $I_{defective}$ is the Raman intensity of the characteristic peaks of Se pre-implanted SiC then irradiated with SHIs and subsequently annealed, while $I_{crystalline}$ is the Raman intensity of the characteristic peaks of pristine SiC, both averaged over the three highly intense peaks (~765 and 791 and 965 cm^{-1}).

The average residual stress in the SiC samples were calculated from LO mode peak shift, according to equation (2) [27]:

$$\omega^{LO} - \omega_0^{LO}(cm^{-1}) = -(4.28 \pm 0.22)\sigma \tag{2}$$

Where ω^{LO} and ω_0^{LO} indicates the Raman shift of the LO mode with (after treatment) and without (before treatment) residual stress, respectively, σ represents the estimated residual stress in GPa and the constant value indicates stress conversion factor of 3C-SiC.

Fig. 3 depicts the RRI of SiC pre-implanted with Se then irradiated with SHIs, as a function of annealing temperature. The RRI serves as a measure of the defect density in the material, with a value of 1 signifying minimal defect and a value of 0 indicating complete disorder or amorphization [28]. This quantitative assessment allows for a more comprehensive understanding of the structural integrity and quality of the SiC following the irradiation and annealing processes. The RRI values of 0.10 and 0.18 were obtained for SiC samples implanted at RT and 350 °C, respectively, after irradiation. This disparity in defect density is further corroborated by the Raman spectra presented in Fig. 2, where the characteristic peaks of as-irradiated sample are notably less pronounced, alongside the presence of the C—C vibration mode. For the RT implanted and then irradiated SiC sample, annealing at 1000 °C yielded an RRI of 0.67, signifying substantial defect recovery, which increased to 0.98 after annealing at 1100 °C. However, at 1200 °C, the RRI dropped to 0.74, indicating a reduction in crystallinity, likely caused by the accumulation of thermally induced stress. In contrast, the 350 °C pre-implanted SiC showed a more gradual healing of defects, with RRI values of 0.36, 0.64 and 0.75 at 1000 °C, 1100 °C, and 1200 °C, respectively. This indicates that recovery is significantly more pronounced in the RT pre-implanted samples compared to those pre-implanted at 350 °C. This difference could be due to increased defect interactions in the RT-implanted samples, where the higher damage levels promote quicker defect recombination during annealing, thus enhancing the recovery process.

The vertical dashed line in Fig. 3 marks the center of the LO mode

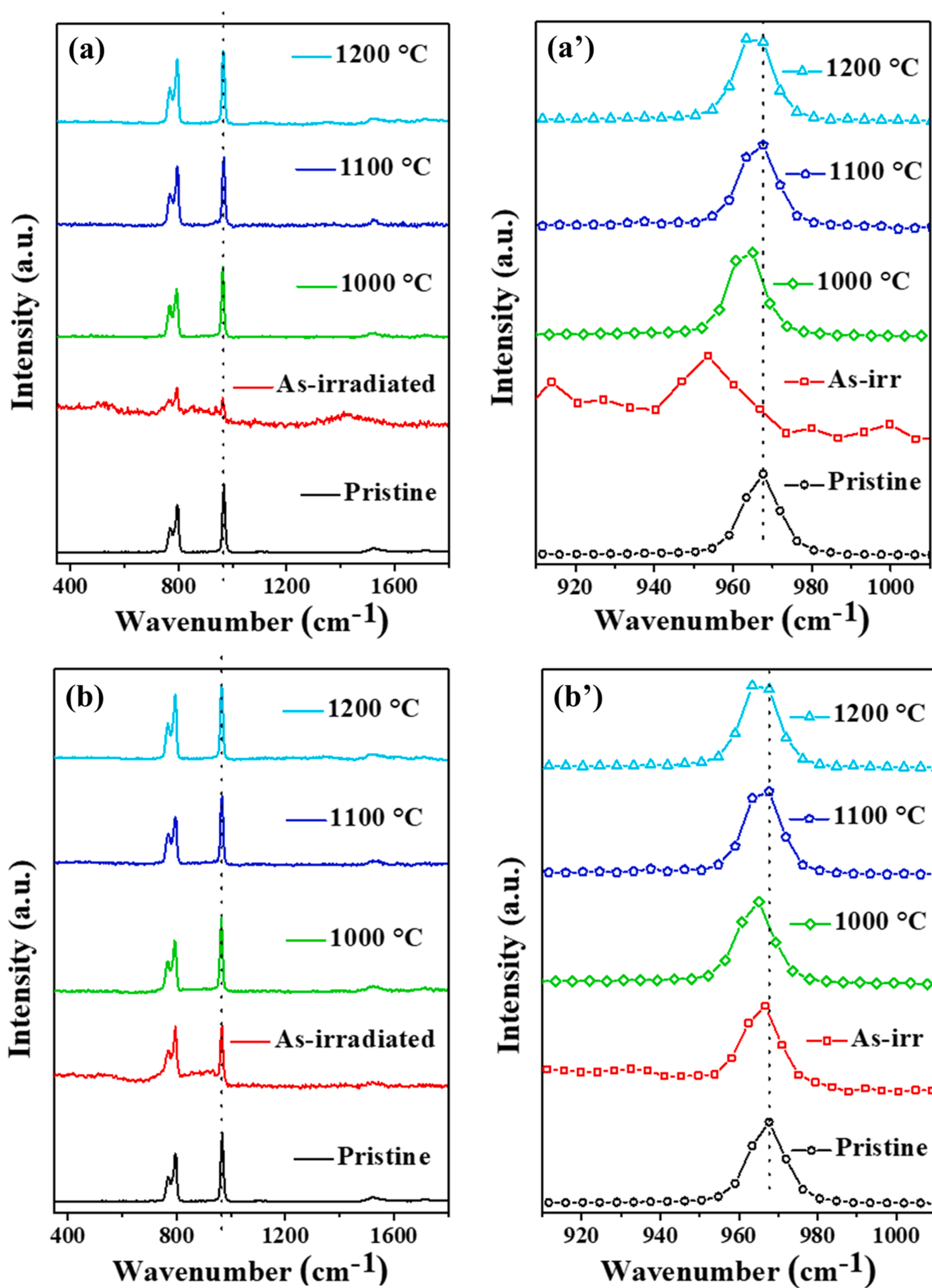

Fig. 2. Raman spectra of the pre-implanted SiC at (a) RT and (b) 350 ℃ then irradiated, subsequently annealed from 1000 to 1200 ℃. The corresponding magnified views of LO peaks are displayed in (a') and (b'), respectively. Pristine and as-irradiated samples were incorporated for comparison purpose.

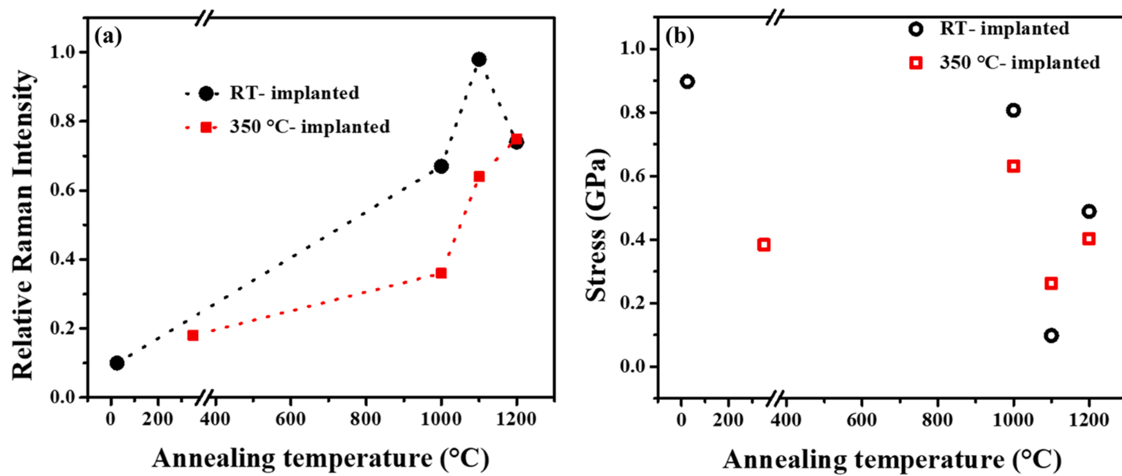

Fig. 3. (a) The relative Raman intensity (RRI) and (b) residual stress (GPa) versus the annealing temperature for SiC pre-implanted at RT and 350 °C, followed by irradiation and annealing between 1000 and 1200 °C. As-irradiated samples are included for comparison.

peak, which served as a reference for monitoring the Raman shift. This shift was subsequently used to estimate the residual stress in the material after treatment. The residual stress measurements revealed values of 0.90 GPa and 0.38 GPa for the RT and 350 °C pre-implanted SiC, subsequently irradiated, respectively. These results suggest modifications in the mechanical properties of the samples, likely due to the elongation of chemical bond lengths compared to those in unstressed crystals [16]. In the RT pre-implanted and irradiated sample, annealing at 1000 °C resulted in a reduction of stress levels to 0.81 GPa. At 1100 °C, the sample reached a nearly stress-free state (~0 GPa), corresponding with an RRI of ~0.98. However, further annealing at 1200 °C reintroduced stress, measured at 0.49 GPa, agreeing well with the measured RRI for the same sample. Annealing the 350 °C pre-implanted and irradiated SiC, annealing at 1000 °C increased the stress to 0.63 GPa, while at 1100 °C, the stress decreased to 0.26 GPa, returning to a level similar to that of the as-irradiated sample after annealing at 1200 °C, indicating complex interplay between thermal treatment, stress evolution, and defect recovery in SiC material.

Fig. 4 and Fig. 5 show SEM micrographs of SiC implanted at RT and 350 °C then irradiated, subsequently annealed sequentially. The SEM surfaces of pristine SiC and RT-only implanted SiC were recently reported by ref [16]. Their findings revealed that the pristine SiC displayed well-pronounced mechanically induced polishing marks, attributed to the polishing process during sample preparation. On the other hand, the RT-only implanted sample exhibited a flat and featureless surface, which was ascribed to sputtering and swelling of the heavily damaged layer caused by low-energy ion bombardment. The SEM micrograph of RT pre-implanted SiC, followed by irradiation, was also recently reported in ref [13]. Their results showed partial visibility of polishing marks re-emerging from the previously featureless and flat surface of the Se-only implanted SiC, indicating the recrystallization of some defects post-irradiation.

Annealing of the RT-implanted and then irradiated samples resulted in more pronounced polishing marks compared to the as-irradiated sample. With clearly visible small grains on the surfaces of 1000 and 1100 ℃ samples, implying that the surface has undergone some level of recrystallization or defect healing. In contrast, the 1200 ℃ sample displayed a rough texture, with tiny thermally induced pores on the surface (see Fig. 4(c)). Comparing these results with unirradiated and annealed samples reported in ref [16], it is evident that recrystallization of defects

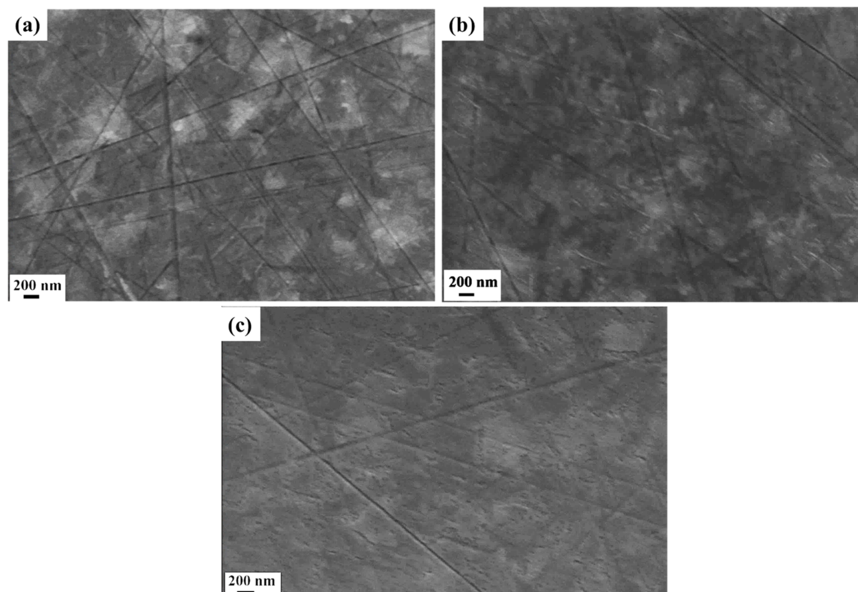

Fig. 4. SEM micrographs of the RT pre-implanted SiC, then irradiated, subsequently sequentially annealed at (a) 1000, (b) 1100 and (c) 1200 ℃.

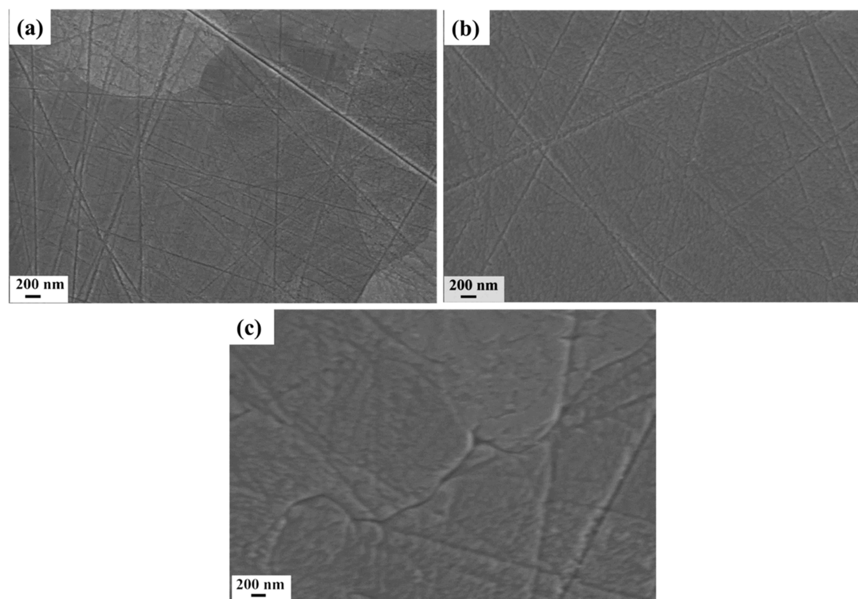

Fig. 5. SEM micrographs of the 350 ℃ pre-implanted SiC, then irradiated, subsequently sequentially annealed at (a) 1000, (b) 1100 and (c) 1200 ℃.

following high temperature annealing is more enhanced in the irradiated samples, which begins after annealing at 1000 ℃, whereas for unirradiated samples only begins at 1100 ℃. This enhancement in recrystallization is due to the thermal spikes generated by electronic energy deposition from the 710 MeV Bi^{51+} ions. Similar surface recrystallization was observed in studies [6–8], where pre-implanted samples were subjected to an electronic energy loss of 20 keV/nm followed by annealing. However, in those studies, annealing up to 1200 °C resulted in surfaces with pores and irregularly shaped crystals. Differences in surface recrystallization between those studies and the current study may be attributed to variations in the chemistry of the implanted species, as well as differences in the maximum electronic energy losses applied. Notably, these surface recrystallization results align with the Raman spectroscopy findings discussed earlier.

The surface of the 350 ℃ implanted SiC, as reported in ref [16], retained polishing marks, although less pronounced compared to the pristine sample. The surface micrographs of Se pre-implanted SiC at 350 ℃, followed by 710 MeV Bi^{51+} irradiation (as-irradiated), were reported in ref [13]. Their results demonstrated that the 710 MeV Bi^{51+} irradiation resulted in more pronounced polishing marks and the appearance of grains, indicating defect recrystallization on the surface. After sequential annealing from 1000 to 1100 ℃, the surfaces of irradiated samples showed large grains with well-defined polishing marks and grain boundaries. Meanwhile, after annealing at 1200 ℃, the grain boundaries began to open. These results clearly highlight the role of 710 MeV Bi^{51+} irradiation in facilitating morphological changes in SiC. A comparison of the 1200 ℃ annealed samples for both unirradiated as reported in ref [16] and irradiated conditions reveals that the grain boundaries remained closed for the unirradiated samples but opened for the irradiated ones, indicating the significant impact of irradiation in enhancing surface modifications.

Se depth profiles from RBS after annealing of the RT and 350 ℃ implanted and then irradiated SiC are shown in Fig. 6, along with their peak positions and retained ratios of the implanted Se as a function of annealing temperature. Sequential annealing the RT implanted then irradiated SiC from 1000 to 1100 °C resulted in no change in the Se implanted depth profiles, accompanied by neither peak shift nor loss. However, annealing up to 1200 °C led to a slight reduction in peak counts, with no considerable peak shift or loss of Se (N.B. the error bars are taken into consideration). This indicates lack of Se migration, with most remaining trapped around the projected range. Meanwhile, for the 350 °C pre-implanted and irradiated samples, annealing between 1000 and 1200 °C also resulted in negligible Se depth profile shift and 100 % Se retention, indicating lack of Se migration as well. Comparing these results to RBS results for the unirradiated samples reported in ref [16], it is clear that the 710 MeV Bi^{51+} irradiation on the RT and 350 °C pre-implanted SiC does not have any significant influence on the transport mechanism of Se, as there was no observed migration in both instances after annealing at the temperatures ranging from 1000 to 1200 °C. The lack of migration or loss of the implanted species in this current study after annealing up to 1200 °C is contrasting the reported migration behavior which was influenced by the structure of Ag and Sr pre-implanted SiC (at RT) then irradiated with 167 MeV Xe ions at RT, whereby the samples were subsequently annealed sequentially from 1100 to 1500 °C [6,8]. In those studies, the migration and loss of the implanted species began after annealing at 1100 °C and increased with higher annealing temperatures, whereas in the current study, annealing up to 1200 °C resulted in negligible migration and loss of the implanted Se. This difference may be attributed to the distinct chemistry of Ag and Sr compared to Se, as well as the initial exposure of the implanted SiC to greater electronic energy loss (33.7 keV/nm) in the present work, which may have altered the SiC structure, thus hindering or halting the migration of the implanted species.

A recent study [13] reported the TEM micrographs of SiC implanted with Se ions at RT and 350 °C, both before and after irradiation with 710 MeV Bi^{51+} ions revealed that Se ion implantation at RT led to the formation of an amorphous layer in SiC of about 187 nm thick from the surface while implantation at 350 °C retained SiC crystal structure with defects. Irradiating with 710 MeV Bi^{51+} ions on the RT implanted samples caused epitaxial recrystallization from the amorphous-crystalline interface accompanied by the appearance of randomly oriented nano-crystallites in the highly defective SiC layer. Irradiation of the SiC pre-implanted at 350 °C exhibited a greater degree of recrystallization compared to SiC pre-implanted at RT.

Fig. 7 shows Bright field (BF) TEM micrographs (a) and (b) and high resolution (HR) (c) of SiC implanted with Se at RT and then irradiated (at RT), subsequently annealed from 1000 °C up to 1200 °C. The selected area diffraction (SAD) patterns taken from both the implanted area and the crystalline bulk are also included in Fig. 7. The featureless (amorphous) layer near the surface corresponds to the protective carbon layer deposited during lamellae preparation. The boundaries between the implanted SiC layer, the crystalline bulk, and/ or the protective carbon

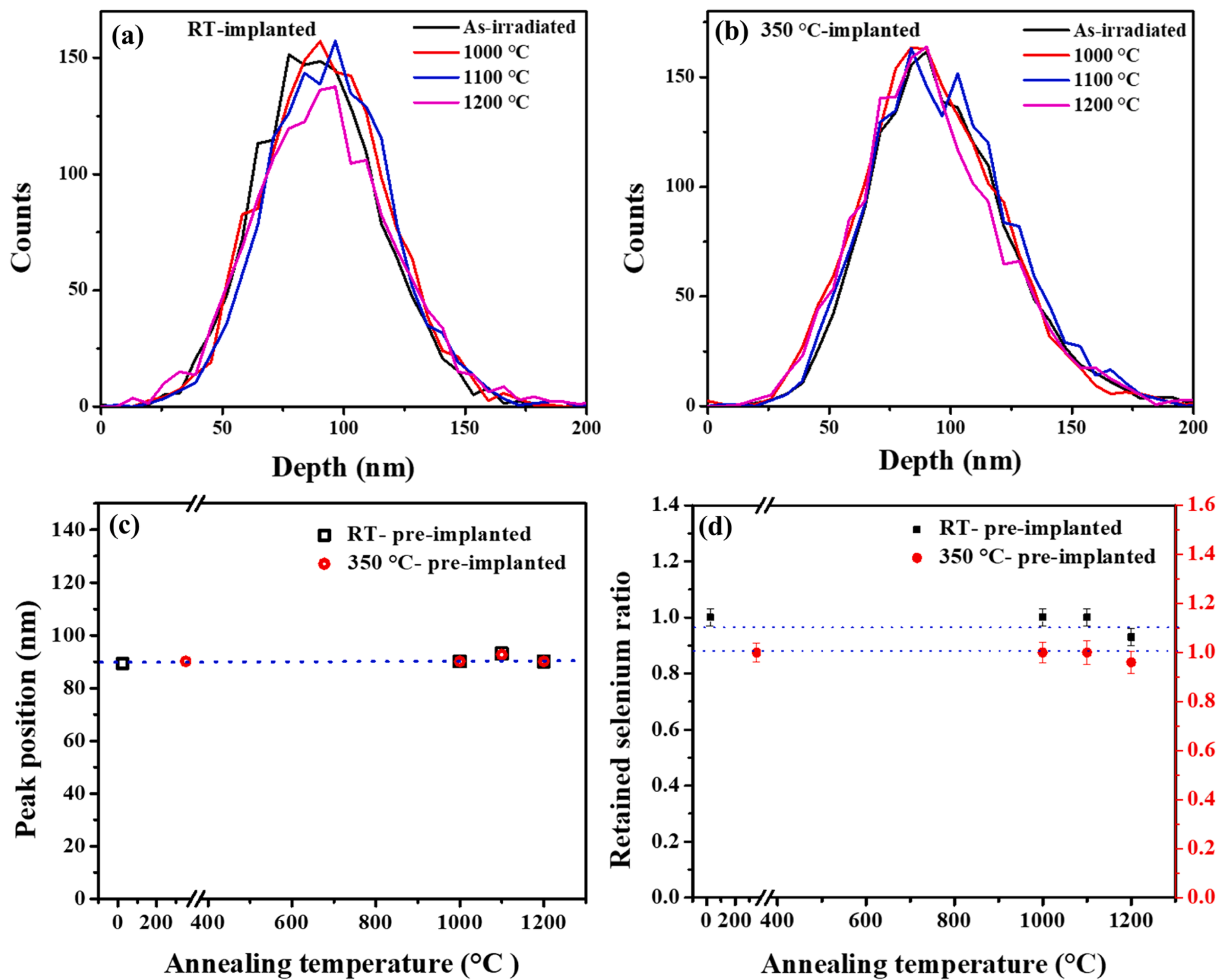

Fig. 6. Se depth profiles from RBS of SiC pre-implanted at (a) RT and (b) 350 °C, then irradiated and annealed at 1000, 1100, and 1200 °C. (c) Se peak position and (d) retained Se as a function of annealing temperature.

coating are indicated by dotted blue lines for clarity. Sequential annealing the sample up to 1200 °C resulted in recrystallization of the former highly defective SiC layer into strained nano-crystalline SiC with cavities (indicated brighter regions- see white circles in Fig. 7(b)) as seen from the BF-TEM micrograph of recrystallized region that is un-even and SAD patterns consisting of rings of multipoint diffractions. Some elongated streaks are also present in the patterns indicating the existence of stacking faults in the recrystallized region. The existence of cavities was expected in the recrystallized amorphous SiC as they are normally observed in the recrystallized former amorphous SiC owing to change in densities and stress [29]. HR-TEM micrograph taken at the damage-crystalline interface (highlighted by a black square in Fig. 7(a)) reveal a highly ordered arrangement of atoms in the implanted region, similar to the crystalline. This confirms the recrystallization of the previously amorphized structure. Moreover, the darker areas in HR image of the implanted region, highlighted by a green circle (see Fig. 7 (c)), indicate the presence of strain in the SiC. The recrystallization after annealing at high temperatures was expected, as the similar effect has been reported for low energy ions pre-implanted SiC (at RT) and then irradiated with 167 MeV Xe^{26+} at RT (maximum electronic energy loss of 20 keV/nm) to fluences of 3.4 × 10^{14} cm $^{-2}$ and 8.4 × 10^{14} cm^{-2}, subsequently annealed at high temperatures [6–8]. Moreover, these findings are consistent with the Raman and SEM results discussed earlier.

Fig. 8 shows the high-angle annular dark-field (HAADF) scanning transmission electron microscopy (STEM) micrograph of the sample sequentially annealed up to 1200 °C together with energy-dispersive X-ray spectroscopy (EDS) elemental mappings of (b) Se, (c) C, and (d) Si. In the HAADF-STEM micrograph, the brighter areas correspond to heavier elements, while the darker regions represent lighter elements and cavities. The bright areas within the defective layer indicate clusters of Se atoms (as seen in Fig. 8(a)). Hence, the varying contrast in the implanted region, confirms the presence of crystallites and cavities. Uneven Se distribution towards the surface is noted, along with the presence of Se precipitates (highlighted with white circles (see Fig. 8(b)), indicating local coalescing of Se atoms. The C and Si atoms are nearly uniformly distributed throughout the defective layer, but regions with C and Si deficiency, possibly due to the formation of precipitates, are also observed (see Fig. 8(c) and (d)). These results align with the absence of Se migration, as indicated by the RBS findings discussed earlier.

Fig. 9 displays BF TEM and HR micrographs of SiC implanted at 350 °C and then irradiated at RT, subsequently annealed from 1000 °C up to 1200 °C. The SAD patterns taken from the implanted area is also included in Fig. 9. Sequential annealing the sample up to 1200 °C resulted in the recrystallization of the previously defective SiC layer into crystalline SiC, though with some minor strained areas. The streak SAD

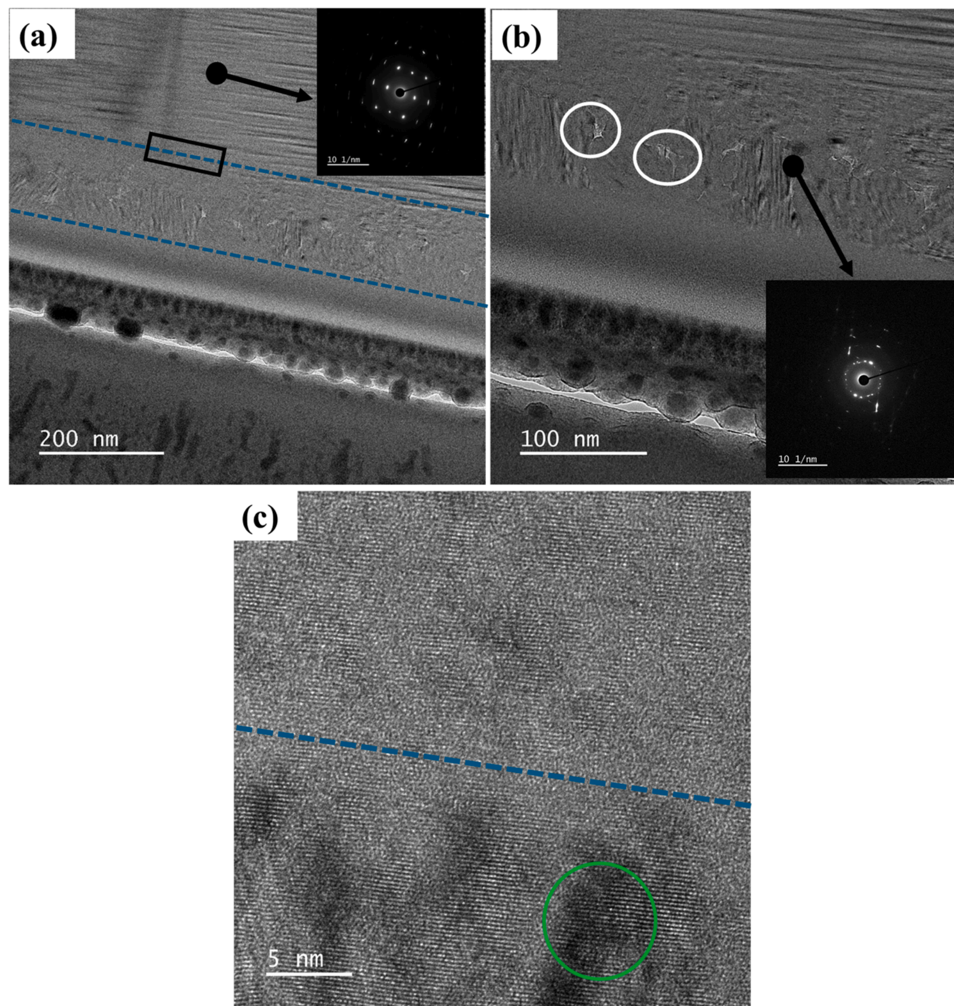

Fig. 7. (a) BF-TEM, (b) higher magnification of (a) and, (c) HR-TEM micrographs of RT pre-implanted SiC then irradiated, subsequently annealed up to 1200 ℃. The arrows point to the selected area diffraction (SAD) patterns captured from the defective and bulk-crystalline region.

patterns from the implanted region indicate the presence of strain or defects. The HR-TEM micrograph taken at the damage-crystalline interface (highlighted by a black square in Fig. 9(a)) reveals a highly ordered arrangement of atoms in the implanted region, similar to those in the crystalline, confirming recrystallization of defects. Moreover, the darker areas in the implanted region (highlighted by a green circle in Fig. 9(b)), indicate the presence of strain in the recrystallized layer. These findings are consistent with the Raman and SEM results discussed earlier.

Fig. 10 shows the HAADF-STEM micrograph of the sample sequentially annealed up to 1200 °C, along with EDS elemental maps for Si, C, and Se. The bright area in the HAADF-STEM image (Fig. 10(a)) confirms the Se-rich implanted region, which is further corroborated by the band observed in the Se elemental map (Fig. 10(b)). Meanwhile, the elemental maps for Si and C indicate that these atoms are uniformly distributed throughout the defective layer (as seen in Fig. 10(c) and (d), respectively).

4. Summary

This work comprehensively investigated the effect of SHIs irradiation and annealing on the microstructural evolution of Se-implanted SiC and transport mechanism of Se ions within the SiC. Polycrystalline SiC was implanted with 200 keV Se ions to fluence of 1×10^{16} cm^{-2} at RT and 350 ℃. Some of these pre-implanted SiC were irradiated with 710 MeV Bi^{51+} ions to fluence of 1×10^{13} cm^{-2} at RT. The pre-implanted then irradiated samples were sequentially annealed under vacuum at temperatures ranging from 1000 to 1200 °C in 100 °C intervals, each for a duration of 10 h. Raman spectroscopy, SEM, and TEM were employed to track the changes in the microstructural formation of SiC, while RBS monitored the migration of Se ions. The findings were compared with those of low energy pre-implanted samples exposed to electronic energy losses of 20 keV/nm, coupled with high-temperature annealing. Sequential annealing of the RT pre-implanted then irradiated sample up to 1200 °C led to a reduction in defects within the previously highly defective SiC layer, transforming it into highly strained nano-crystalline SiC with cavities. This process also resulted in a highly ordered atomic arrangement in the implanted region, similar to that observed in crystalline SiC, thereby confirming recrystallization. Annealing up to 1200 °C also resulted in Se precipitate formation. In contrast, annealing the 350 °C pre-implanted then irradiated sample up to 1200 °C produced nano-crystalline SiC, with minor strained regions. The recrystallization was further confirmed by a highly ordered atomic arrangement in the implanted region, similar to that of crystalline SiC. SEM and Raman analyses corroborated the significant recrystallization observed in both RT and 350 °C pre-implanted, then irradiated SiC samples, subsequently annealed sequentially. RBS depth profiling revealed that annealing both RT and 350 °C pre-implanted, subsequently irradiated samples up to 1200 °C resulted in insignificant loss and migration of the implanted Se. Comparing these results to those from samples exposed to 20 keV/nm electronic energy losses and annealing, the study suggests that both the chemistry of the implanted species and the level of electronic energy loss

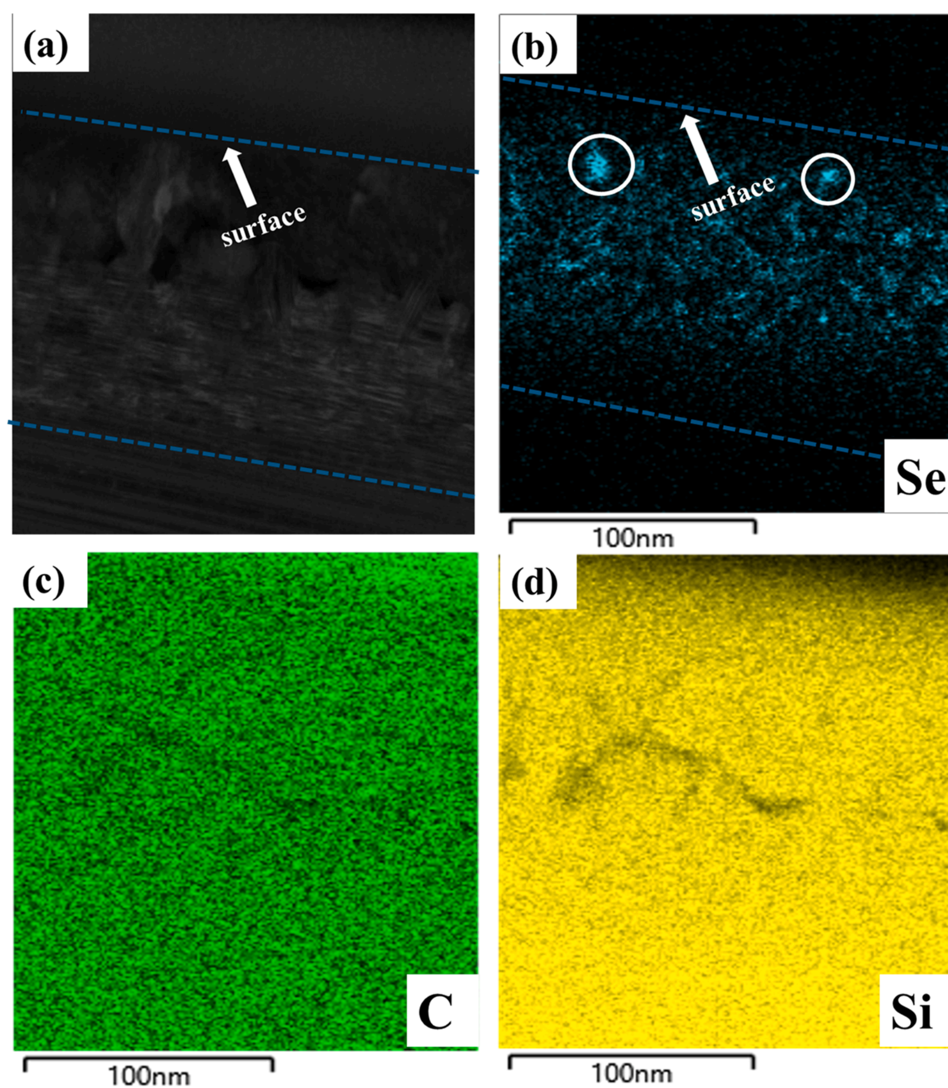

Fig. 8. (a) HAADF-STEM micrograph of RT pre-implanted SiC then irradiated, subsequently sequentially annealed up to 1200 °C for 10 h and EDS maps of (b) Se, (c) C, and (d) Si. The arrows in (a) and (b) indicates the surface of the material.

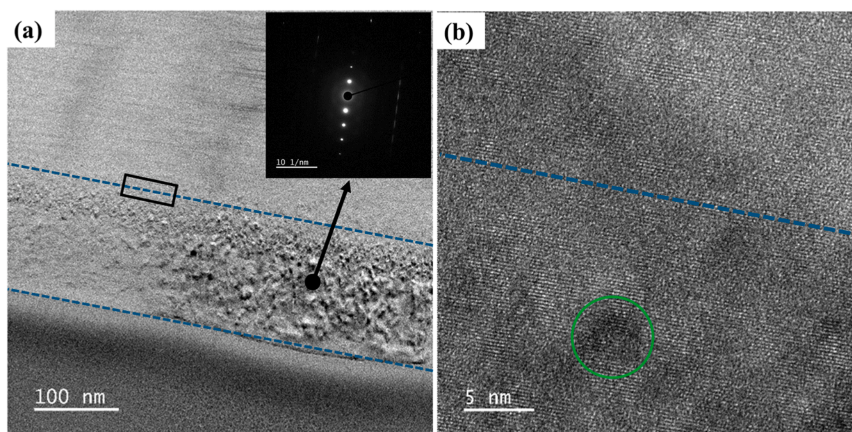

Fig. 9. (a) BF-TEM and (b) HR-TEM micrographs of 350 °C pre-implanted SiC then irradiated, subsequently sequentially annealed up to 1200 °C. The arrow points to the selected area diffraction (SAD) patterns captured from the defective region.

impact the SiC structure and the migration of the implants. These findings deepen our understanding of the microstructural evolution of Se pre-implanted SiC and transport dynamics of Se within SiC, which could enhance the safety of modern nuclear reactors.

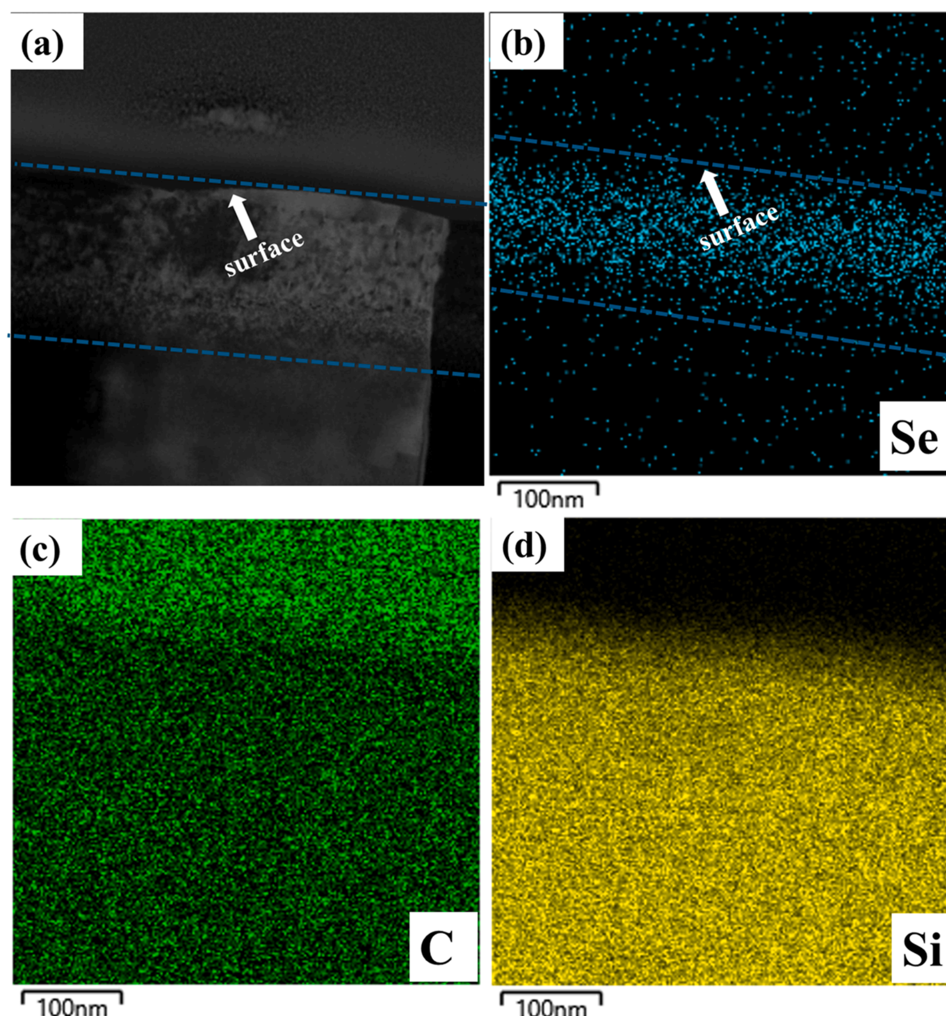

Fig. 10. (a) HAADF-STEM micrograph of 350 °C pre-implanted SiC then irradiated, subsequently annealed up to 1200 °C for 10 h and EDS maps of (b) Se, (c) C, and (d) Si. The arrows in (a) and (b) indicates the surface of the material.

CRediT authorship contribution statement

T.S. Mabelane: Writing – original draft, Visualization, Methodology, Investigation, Formal analysis, Data curation, Conceptualization. **Z.A.Y. Abdalla:** Conceptualization, Data curation, Validation, Writing – review & editing. **V.A. Skuratov:** Conceptualization, Resources. **S.S. Ntshangase:** Data curation, Resources, Visualization. **S.C. Masikane:** Data curation, Resources, Visualization. **T.T. Hlatshwayo:** Conceptualization, Funding acquisition, Methodology, Project administration, Resources, Supervision, Validation, Writing – review & editing.

Declaration of competing interest

The authors declare that they have no known competing financial interests or personal relationships that could have appeared to influence the work reported in this paper.

Acknowledgements

Financial support by the National Research Foundation (NRF) of South Africa (Grant numbers: 122894, 120471 and 2204072593) is gratefully acknowledged.

Data availability

Data will be made available on request.

References

[1] J.B. Malherbe, Topical review: diffusion of fission products and radiation damage in SiC, J. Phys. D Appl. Phys. 4647 (2013) 473001.
[2] P. Hosemann, J.N. Martos, D. Frazer, G. Vasudevamurthy, T.S. Byun, J.D. Hunn, B. C. Jolly, K. Terrani, M. Okuniewski, Mechanical characteristics of SiC coating layer in TRISO fuel particles, J. Nucl. Mater. 442 (2013) 133.
[3] Y. Goldberg, M. Levinshtein, S. Rumyantsev, Silicon Carbide (SiC), Properties of Advance Semiconductor Materials, Wiley, 2001.
[4] N.G. van der Berg, J.B. Malherbe, A.J. Botha, E. Friedland, Thermal etching of SiC, Appl. Surf. Sci. 258 (2012) 5561.
[5] Y. Katoh, L.L. Snead, I. Szlufarska, W.J. Weber, Radiation effects in SiC for nuclear structural applications, Curr. Opin. Solid State Mater. Sci. 16 (3) (2012) 143.
[6] H.A.A. Abdelbagia, V.A. Skuratov, S.V. Motloung, E.G. Njoroge, M. Mlambo, J. B. Malherbe, J.H. O'Connell, T.T. Hlatshwayo, Effect of swift heavy ions irradiation in the migration of silver implanted into polycrystalline SiC, Nucl. Inst. Methods Phys. Res. B. 461 (2019) 201.
[7] H.A.A. Abdelbagi, V.A. Skuratov, S.A. Adeojo, T.M. Mohlala, T.T. Hlatshwayo, J. B. Malherbe, Effect of SHI irradiation and high temperature annealing on the microstructure of SiC implanted with Ag, Nucl. Instrum. Methods Phys. Res., Sect B. 511 (2022) 18.
[8] H.A.A. Abdelbagi, V.A. Skuratov, S.V. Motloung, E.G. Njoroge, M. Mlambo, T. T. Hlatshwayo, J.B. Malherbe, Effect of swift heavy ions irradiation on the migration behavior of strontium implanted into polycrystalline SiC, Nucl. Instr. Meth. Phys. Res. Sect. B. 451 (2019) 113.
[9] T.T. Hlatshwayo, J.H. O'Connell, V.A. Skuratov, M. Msimanga, R.J. Kuhudzai, E. G. Njoroge, J.B. Malherbe, Effect of Xe ion (167 MeV) irradiation on polycrystalline SiC implanted with Kr and Xe at room temperature, J. Phys. D 48 (2015) 465306.

[10] T.T. Hlatshwayo, J.H. O'Connell, V.A. Skuratov, E. Wendler, E.G. Njoroge, M. Mlambo, J.B. Malherbe, Comparative study of the effect of swift heavy ion irradiation at 500 ℃ and annealing at 500 ℃ on implanted silicon carbide, RSC Adv. 6 (2016) 68593.
[11] A. Benyagoub, A. Audren, L. Thomé, F. Garrido, Athermal crystallization induced by electronic excitations in ion-irradiated silicon carbide, Appl. Phys. Lett. 89 (2006) 241914.
[12] A. Benyagoub, A. Audren, Mechanism of the swift heavy ion induced epitaxial recrystallization in pre-damaged silicon carbide, J. Appl. Phy. 106 (2009) 08351.
[13] T.S. Mabelane, M. Sall, Z.A.Y. Abdalla, V.A. Skuratov, T.T. Hlatshwayo, Effect of 710 MeV Bi^{51+} swift heavy ions irradiation on Se pre-implanted polycrystalline SiC, Vac 224 (2024) 113189.
[14] W. Jiang, W.J. Weber, Y. Zhang, S. Thevuthasan, V. Shutthanandan, Ion beam analysis of irradiation effects in 6H–SiC, Nucl. Instrum. Methods Phys. Res B. 207 (2003) 92.
[15] A. Audren, A. Benyagoub, L. Thome, F. Garrido, Ion implantation of iodine into silicon carbide: influence of temperature on the produced damage and on the diffusion behaviour, Nucl. Instr. Meth. Phys. Res. B. 266 (2008) 2810.
[16] Z.A.Y. Abdalla, M.Y.A. Ismail, E.G. Njoroge, E. Wendler, J.B. Malherbe, T. T. Hlatshwayo, Effect of heat treatment on the migration behaviour of selenium implanted into polycrystalline SiC, Nucl. Inst. Methods Phys. Res. B. 487 (2021) 30.
[17] P. Bienvenu, P. Cassette, G. Andreoletti, M.M. Bé, J. Comte, M.C. Lépy, A new determination of 79Se half-life, App. Rad. Iso. 65 (3) (2007) 355.
[18] B. Ma, M. Kang, Z. Zheng, F. Chen, J. Xie, L. Charlet, C. Liu, The reductive immobilization of aqueous Se (IV) by natural pyrrhotite, J. Harz. Mat. 276 (2014) 422.
[19] Argonne National Laboratory, EVS Human Health Fact Sheet, 2005. August.
[20] Z.A.Y. Abdalla, E.G. Njoroge, M. Mlambo, S.V. Motloung, J.B. Malherbe, T. T. Hlatshwayo, Isothermal annealing of selenium (Se)-implanted silicon carbide: structural evolution and migration behavior of implanted Se, Mat. Chem. Phys. 276 (2022) 12533.
[21] Z.A.Y. Abdalla, M.Y.A. Ismail, E.G. Njoroge, T.T. Hlatshwayo, E. Wendler, J. B. Malherbe, Migration behaviour of selenium implanted into polycrystalline 3C–SiC, Vacu 175 (2020) 109235.
[22] E. Friedland, J.B. Malherbe, N.G. van der Berg, T. Hlatshwayo, A.J. Botha, E. Wendler, W. Wesch, Study of silver diffusion in silicon carbide, J. Nucl. Mater. 389 (2009) 326.
[23] M.J. Madito, T.T. Hlatshwayo, C.B. Mtshali, Chemical disorder of a-SiC layer induced in 6H-SiC by Cs and I ions co-implantation: raman spectroscopy analysis, Appl. Surf. Sci. 538 (2021) 148099.
[24] M. Toulemonde, Ch. Dufour, A. Meftah, E. Paumier, Transient thermal processes in heavy ion irradiation of crystalline inorganic insulators, Nucl. Instrum. Methods Phys. Res. B 166-167 (2000) 903.
[25] H. Dammak, A. Dunlop, D. Lesueur, Tracks in metals by MeV Fullerenes, Phys. Rev. Lett. 74 (7) (1995) 1135.
[26] S. Sorieul, J.M. Costantini, L. Gosmain, L. Thom' e, J.J. Grob, Raman spectroscopy study of heavy-ion-irradiated α-SiC, J. Phys. Condens. Matter. 18 (22) (2006) 5235.
[27] Z. Xu, Z. He, Y. Song, X. Fu, M. Rommel, X. Luo, A. Hartmaier, J. Zhang, F. Fang, Topic review: application of Raman spectroscopy characterization in micro/nano-machining, Micromachines 9 (7) (2018) 361.
[28] T. Mokgadi, Z. Abdalla, H. Abdelbagi, M. Msimanga, C. Maepa, V. Skuratov, T. Hlatshwayo, Helium and strontium co-implantation into SiC at room temperature and isochronal annealing: structural evolution of SiC and migration behaviour of strontium, Mater. Chem. Phys. 294 (2022) 126998.
[29] A. Höfgen, V. Heera, F. Eichhorn, W. Skorupa, Annealing and recrystallization of amorphous silicon carbide produced by ion implantation, J. Appl. Phys. 84 (9) (1998) 4769.